Sohag Journal of Mathematics
An International Journal

http://dx.doi.org/10.18576/sjm/120202

Impact of Cross Diffusion on MHD Flow of Casson-Williamson Nanofluid Past a Reactive Nonlinear Stretching Surface With Thermal Radiation

Christian J. Etwire[1] *and Fuseini J. Mathias* [1,*]

[1]Department of Mathematics, School of Mathematical Sciences, C. K. Tedam University of Technology and Applied Sciences, P.O. Box 24, Navrongo, Ghana

Received: 27 Nov. 2024, Revised: 4 Feb. 2025, Accepted: 24 Mar. 2025
Published online: 1 May 2025

Abstract: In this study, we investigate the impact of cross-diffusion on the magnetohydrodynamics (MHD) flow of Casson-Williamson nanofluid over a reactive nonlinear stretching surface under the influence of thermal radiation.The mathematical model which interfused thermal-diffusion, diffusion-thermo and radiation effects are formulated as partial differential equations. These equations are transformed into coupled nonlinear ordinary differential equations using similarity variables and subsequently solved using the fourth-order Runge-Kutta method combined with the Newton-Raphson shooting technique. A comparison of the Nusselt number result with existing literature shows excellent agreement, validating the accuracy of the model. The results found the Dufour number and radiation parameter to appreciate the temperature distribution of both Casson and Williamson nanofluids with temperature been significantly strengthened for Casson nanofluid.This suggests that Casson nanofluid is highly effective in heat storage applications such as accumulators and solar panels, whereas Williamson nanofluid, with its higher skin friction coefficient, is eminent for the formulation of brake and automatic transmission fluids.

Keywords: Diffusion, Nonlinear,Reactive, Radiation, Soret

1 Introduction

The influence of cross-diffusion on the behaviour of magnetized Casson-Williamson nanofluids, especially under the effects of thermal radiation and reactive surfaces, has attracted growing interest due to its diverse practical applications in both natural and artificial phenomena. Cross-diffusion enhances temperature and concentration gradients, leading to improved thermal regulation and solute distribution in the fluid. Thermal radiation further amplifies this effect by intensifying energy transport, modifying viscosity variations, and influencing the nanofluids overall stability. These interactions are particularly valuable in complex systems requiring specialized flow properties. In heat transfer applications, they enable precise temperature control, while in material science, they contribute to enhanced thermal processing techniques. The interplay of cross-diffusion and thermal radiation enhances efficiency in industrial applications, including drilling, polymer production and thermal energy management. Additionally, their role in magnetohydrodynamics (MHD) extends to advanced applications like coating technologies, lubricating systems and wastewater treatments, demonstrating the synergy between theoretical research and real-world innovations. The choice of Williamson model alongside with the Casson fluid is due to their distinct yet complementary rheological characteristics, which provide a broader understanding of non-Newtonian nanofluid behaviour. The Casson model accounts for yield stress effects and is particularly suitable for characterizing shear-thinning fluids with structural rigidity, such as blood and polymer suspensions. The Williamson model also exhibits shear-thinning behaviour without a yield stress, making it relevant for low-viscosity polymeric and biofluid applications. By considering both models, a comprehensive analysis of nanofluid dynamics is achieved, facilitating better predictions of flow resistance, heat transfer efficiency and stability under MHD and

* Corresponding author e-mail: fuseinijohnmathias8@gmail.com

thermal radiation effects. [1] researched heat and fluid flow owing to non-linearly stretched surfaces and discovered the nonlinear parameter to affect the surface temperature. [2] examined the influence of radiation on MHD flow across a vertical plate under convective boundary conditions. It was found that the Biot number improved the skin friction coefficient, heat transmission, and plate surface temperature. [3] analyzed the effects of non-linear thermal radiation on slip flow and heat of fluid particle suspension containing nanoparticles across a nonlinear stretching sheet immersed in a porous medium. The velocity of fluid and dust phases decreased when slip and permeability parameters increased. [4] employed a revised thermal flux model to discuss magnetohydrodynamics flow of viscoelastic liquid and found the fractional parameter to affect the velocity and temperature profiles. [5] examined the role of non-linear thermal radiation and non-uniform heat source on the flow of a Casson nanofluid with Brownian motion and chemical reaction. The non-uniform heat source parameter was discovered to increase the temperature and thermal boundary layer thickness. [6] examined the effects of Chemical reaction and thermal radiation on magnetohydrodynamics flow of Casson -Williamson nanofluid over a porous stretching surface and observed the Williamson Parameter to reduce the velocity of the nanofluid. [7] investigated the impact of thermal stratification on the magnetic flow of electrically induced Maxwell nanofluid over a reactive stretching plate. The Richardson number was observed to increase the thickness of the momentum boundary layer while it decreased the thicknesses of the thermal and solutal boundary layers. [8] employed enhanced Cattaneo-Christov heat and mass fluxes to study thermo-solutal time relaxation effect on mixed convection flow of Carreau fluid. The investigation found the performance of the thermo-relaxation factor in the temperature field and the solutal relaxation factor in the concentration field to decline. [9] studied the behaviour of hybrid nanofluid and stagnation point flow towards a stretched surface with melting heat transfer and second order slip. [10] investigated heat transport enhancement in time-independent ternary hybrid nanofluid flow over a linear and nonlinear stretching surface with thermal radiation. [11] provided a unique fractional constitutive model for evaluating the behaviour of buoyancy-driven flow and heat transfer. The study found the thermal fractional parameter to increase the heat transfer rate by 8 %. [12] established convective conditions for magnetohydrodynamic non-Newtonian nanofluid flow with nonlinear thermal radiation and heat absorption. [13] investigated heat transmission from nanofluid movement impinging on a porous extending sheet. The radiation parameter was found to increase the temperature boundary layer thickness. [14] examined the role of copper nanoparticles on water and silicone flow over radially stretching sheet. Platelet-shaped nanoparticles exhibited the highest skin friction coefficient, while blade-shaped nanoparticles had the lowest skin friction coefficient. [15] investigated the heat and mass transport properties of a non-Newtonian Casson-Williamson nanofluid flow over a porous stretched sheet. The skin-friction coefficient was noted to increase with the porosity parameter. [16] analyzed the flow of water and engine oil-based nanofluids and the impact of viscous dissipation and varied viscosity on a stretching surface. The temperature field was found to increase with the heat source and dynamic viscosity parameters. [17] studied the effect of heat generation and thermal radiation on Eyring-powell hybrid nanofluid flow across a stretched surface.The study observed the hybrid nanofluid density and dynamic viscosity to increase with the volume fraction. [18] studied the heat and mass transport characteristics of thermally radiated bi-directional slip flow over a permeable stretched surface. [19] investigated the effect of chemical reaction and cross diffusion on heat and mass transfer properties of a viscoelastic oil-based nanofluid on a porous nonlinear stretching surface. The study discovered that CuO oil-based nanofluid had a higher mass transfer rate than Al_2O_3-oil-based nanofluid under the same viscoelastic conditions. [20] investigated the impact of non-uniform heat generation on the flow of magnetized Casson-Williamson nanofluid towards a dissipative stagnation point. The findings revealed that the magnetic field parameter greatly influenced the velocity, temperature and concentration distributions. The literature perused provide limited insight into the complex flow behaviour of Casson-Williamson nanofluids under various transport dynamics. Thus, this study investigates the effect of cross diffusion on MHD flow of Casson-Williamson nanofluid across a reactive nonlinear stretching surface with thermal radiation. This research finds prominence in biomedical, petroleum and chemical industries.

2 Mathematical Model

Consider laminar,incompressible, two-dimensional flow of a viscous, electrically conducting, and radiating Casson-Williamson nanofluid across a chemically reactive non-linear stretching surface. The flow is restricted to the xy axes and is subjected to thermal-diffusion and diffusion-thermo effects. The y-axis is normal to the stretching surface, whereas the x-axis is along it.The velocity of the stretching sheet is $u_w = ax^m$, where $a > 0$ is a constant and m represents the sheet's nonlinearity. A homogeneous transverse magnetic field of intensity Bo is induced parallel to the y-axis. The induced external magnetic and electric fields are assumed to be minimal $(Fig.1)$. Based on the boundary layer and Rosseland approximations, and taking

$$\tau_{ij} = \mu \left(\left(1 + \frac{1}{\beta} \right) \frac{\partial u}{\partial y} + \frac{\Gamma}{\sqrt{2}} \left(\frac{\partial u}{\partial y} \right)^2 \right)$$

to represent the shear stress of the Casson-Williamson nanofluid, the flow equations can be stated as follows [6]:

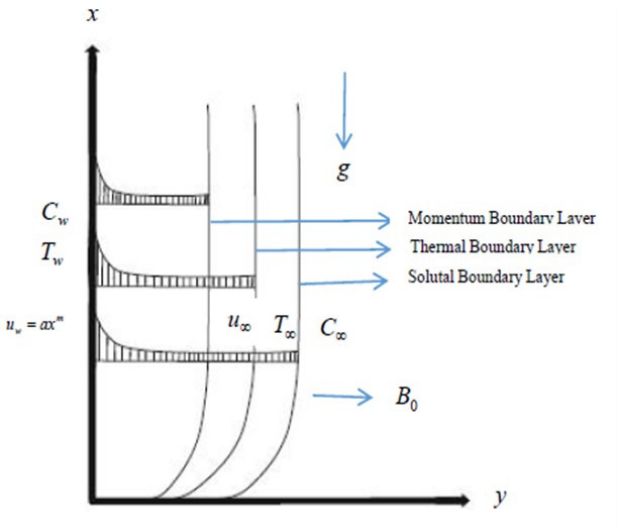

Fig. 1: Schematic diagram of the flow problem.

$$\frac{\partial u}{\partial x}+\frac{\partial v}{\partial y}=0 \tag{1}$$

$$u\frac{\partial u}{\partial x}+v\frac{\partial u}{\partial y}=\nu\left(1+\frac{1}{\beta}\right)\frac{\partial^2 u}{\partial y^2}+\sqrt{2}\nu\Gamma\frac{\partial u}{\partial y}\frac{\partial^2 u}{\partial y^2} +g\beta_T(T-T_\infty)+g\beta_c(C-C_\infty)-\frac{\sigma B_o^2}{\rho}u \tag{2}$$

$$u\frac{\partial T}{\partial x}+v\frac{\partial T}{\partial y}=\frac{k}{\rho c_p}\left(1+\frac{16\sigma^* T_\infty^3}{3kk^*}\right)\frac{\partial^2 T}{\partial y^2} +\frac{\mu}{\rho c_p}\left[\left(1+\frac{1}{\beta}\right)\left(\frac{\partial u}{\partial y}\right)^2+\frac{\Gamma}{\sqrt{2}}\left(\frac{\partial u}{\partial y}\right)^3\right] +\tau\left(D_B\frac{\partial C}{\partial y}\frac{\partial T}{\partial y}+\frac{D_T}{T_\infty}\left(\frac{\partial T}{\partial y}\right)^2\right)+\frac{D_m\kappa_t\partial^2 C}{c_s c_p\partial y^2} \tag{3}$$

$$u\frac{\partial C}{\partial x}+v\frac{\partial C}{\partial y}=D_B\frac{\partial^2 C}{\partial y^2}+\frac{D_T}{T_\infty}\frac{\partial^2 T}{\partial y^2}+\frac{D_m\kappa_t}{T_m}\frac{\partial^2 T}{\partial y^2}-\gamma(C-C_\infty) \tag{4}$$

The x and y components of velocity are denoted by u and v, respectively, and σ represents electrical conductivity. g is the acceleration due to gravity, β signifies the Casson parameter. Γ is the Williamson parameter, B_o is the uniform magnetic field, and k is the permeability term. D_B represents the Brownian diffusion coefficient. β_c refers to the coefficient of solutal expansion. β_T coefficient of thermal expansion, c_s indicates concentration susceptibility of the nanofluid, c_p represents the specific heat capacity at constant pressure. T_∞ represents the free stream temperature. τ is the ratio of the nanoparticle material's effective heat capacity to that of the fluid and D_T is the thermal diffusion coefficient, γ is the reaction rate, C is the species concentration, C_∞ is the free stream concentration. D_m is the mean diffusion coefficient, T_m is the mean temperature of the nanofluid, ρ is the fluid density, μ is the dynamics viscosity, ν is the kinematic viscosity, and T is the temperature.
The boundary conditions on the surface of the plate at $y=0$ are:

$$u(x,0)=bx^m, v(x,0)=0, T(x,0)=T_w, C(x,0)=C_w. \tag{5}$$

The boundary conditions far away from the surface of the plate as $y\to\infty$ are;

$$u(x,\infty)\to 0, T(x,\infty)\to T_\infty, C(x,\infty)\to C_\infty \tag{6}$$

2.1 *Similarity Transformation*

The stream function $\psi(x,y)$ is defined in the usual way as:

$$u=\frac{\partial\psi}{\partial y}\text{and v}=-\frac{\partial\psi}{\partial x} \tag{7}$$

Equation (7) satisfies the continuity equation (1) exactly. To find a similarity solution for equations $(2)-(4)$, define an independent dimensionless variable, η, a stream function, ψ, in terms of a dependent variable, $f(\eta)$, a dimensionless concentration, (ϕ), and a dimensionless temperature, $\theta(\eta)$, as follows:

$$\eta=y\sqrt{\frac{b(m+1)}{2\nu}}x^{\frac{m-1}{2}},\quad \psi=\sqrt{\frac{2b\nu}{m+1}}x^{\frac{m+1}{2}}f(\eta), \quad \theta(\eta)=\frac{T-T_\infty}{T_w-T_\infty}, \phi(\eta)=\frac{C-C_\infty}{C_w-C_\infty}. \tag{8}$$

Substituting the appropriate terms into equations (2)–(4) yield the coupled nonlinear differential equations as;

$$\left(1+\frac{1}{\beta}\right)f'''(\eta)-\frac{2m}{m+1}f'^2(\eta)+f(\eta)f''(\eta)+Wef''(\eta)f'''(\eta) +\frac{2}{m+1}G_T\theta(\eta)+\frac{2}{m+1}G_c\phi(\eta)-\frac{2}{m+1}Mf'(\eta)=0 \tag{9}$$

$$(1+R)\theta''(\eta)+Prf(\eta)\theta'(\eta)+Ec\left(\left(1+\frac{1}{\beta}\right)f''^2(\eta)+\frac{We}{2}f''^3(\eta)\right) +Pr\left(N_b\theta'(\eta)\phi'(\eta)+N_t\theta'^2(\eta)\right)+PrD_0\phi''(\eta)=0 \tag{10}$$

$$\phi''(\eta)+Scf(\eta)\phi'(\eta)+\frac{N_t}{N_b}\theta'''(\eta)+ScS_O\theta'''(\eta)-\frac{2}{m+1}Sc\omega_1\phi(\eta)=0 \tag{11}$$

subject to the boundary conditions

$$f(x)=0, f'(0)=1, \theta(0)=1, \phi(0)=1, \text{at}(\eta)=0 \tag{12}$$

$$f'(\infty)\to 0, \theta(\infty)\to 0, \phi(\infty)\to 0, \text{as}(\eta)\to\infty \tag{13}$$

The prime symbol represents differentiation with regards to η. $Ec=\frac{\mu b^2x^{2m}}{\kappa(T_w-T_\infty)}$ represents the Eckert number, and

$Pr = \frac{\nu}{\alpha}$ represents the Prandtl number, $We = \Gamma x^{\frac{3m-1}{2}} \sqrt{\frac{b^3(m+1)}{\nu}}$ represents the Wesseinberg number, $Nb = \frac{D_B \tau (C_w - C_\infty)}{T_\infty \nu}$ represents the Brownian motion parameter, $N_t = \frac{D_T \tau (T_w - T_\infty)}{T_\infty \nu}$ represents the thermophoresis parameter, $D_0 = \frac{D_m \kappa_t (C_w - C_\infty)}{C_s C_p \nu (T_w - T_\infty)}$ represents the Dufour number, $R = \frac{16\sigma^* T_\infty^3}{3\kappa\kappa^*}$ is the radiation parameter, $G_T = \frac{g\beta_T (T_w - T_\infty)}{u_\omega^2} x$ is the thermal Grashof number, $G_c = \frac{g\beta_c (C_w - C_\infty)}{u_\omega^2} x$ is the solutal Grashof number, $M = \frac{\sigma \beta_0^2}{\rho b x^{m-1}}$ represents the magnetic field parameter, $Sc = \frac{\nu}{D_B}$ is the Schmidt number, $S_o = \frac{D_m \kappa_t (T_w - T_\infty)}{T_m \nu (C_w - C_\infty)}$ represents the Soret number and $\omega_1 = \frac{\gamma}{b x^{m-1}}$ represents the rate of chemical reaction.

Parameters of engineering interest are the skin friction coefficient (Cf), Nusselt number (Nu), and Sherwood number, which are defined as follows:

$$C_f = \frac{\tau_w}{\rho u_w^2}, , Nu = \frac{x q_w}{\kappa (T_w - T_\infty)}, Sh = \frac{x q_m}{D_B (C_w - C_\infty)} \tag{14}$$

Where τ_w is the wall shear stress, q_w is the wall heat flux, and q_m is the wall mass flux, which are respectively defined as;

$$\begin{aligned} \tau_w &= \mu \left[\left(1 + \frac{1}{\beta}\right) \frac{\partial u}{\partial y} + \frac{\Gamma}{\sqrt{2}} \left(\frac{\partial u}{\partial y}\right)^2 \right]_{y=0}, \\ q_w &= -\kappa \left(1 + \frac{16\sigma^* T_\infty^3}{3\kappa\kappa^*}\right) \left.\frac{\partial T}{\partial y}\right|_{y=0}, \\ q_m &= -D_B \left.\frac{\partial C}{\partial y}\right|_{y=0} \end{aligned} \tag{15}$$

Substituting equations (12) and (13) into (14) and (15) yields;

$$Cf_x = \sqrt{\frac{m+1}{2Re}} \left(\left(1 + \frac{1}{\beta}\right) f''(0) + \frac{We}{2} f''^2(0) \right) \tag{16}$$

$$Nu = -\sqrt{\frac{(m+1)Re}{2}} (1+R)\theta'(0) \tag{17}$$

$$Sh = -\sqrt{\frac{(m+1)Re}{2}} \phi'(0) \tag{18}$$

3 Results and Discussions

The coupled nonlinear differential equations $(9-11)$, as well as the boundary conditions $(12-13)$, are numerically solved using the fourth-order Runge-Kutta method and Newton Raphson shooting technique. MAPLE software suite was used to generate numerical and pictorial results. The thermophysical parameters used in this study are the magnetic field parameter (M), soret number (S_o), thermal grashof number (G_T), solutal grashof number (G_c), the Prandtl number (Pr), the thermophoresis parameter (N_t), Brownian motion parameter, (N_b), nonlinear parameter (m), Schmidt number (Sc), Eckert number (Ec), Radiation parameter (R), Rate of chemical reaction parameter (ω_1) and Dufour number (D_o). For numerical and graphical results, black font colour signifies Williamson nanofluid and blue font colour represents Casson nanofluid.

3.1 Validation of the Flow Model

The results of the present model for the local Nusselt number represented by $(-\theta(0))$ were compared with the work of [1] for varied values of the Prandtl number (Pr) and nonlinear stretching parameter (m) and for $G_c = G_T = N_t = N_b = Sc = Ec = R = M = S_o = D_o = \omega_1 = 0$. The excellent agreement with the results of [1] up to four decimal places validates the existing numerical method. Table 1 summarizes the contrast.

Table 1: Computations indicating comparison with [1]

		[1]	**Present Work**
Pr	m	-$\theta'(0)$	-$\theta'(0)$
1.0	0.2	0.610262	0.610216
	0.5	0.595277	0.595224
	1.5	0.574537	0.574771
5.0	0.2	1.607175	1.607784
	0.5	1.586744	1.586779
	1.5	1.557463	1.557691

3.2 Numerical Results

Table 2: Computations showing $-f''(0)$, $-\theta'(0)$, and $-\phi(0)$ for different parameter values.

S_o	Sc	N_b	N_t	R	ω_1	m	G_T	G_c	M	D_0	Pr	Ec	$-f''(0)$	$-\theta'(0)$	$-\phi(0)$
0.1	0.5	0.5	0.2	0.5	0.1	1.1	0.1	0.1	0.1	0.1	3	0.1	1.098293	0.632291	0.246583
													0.525733	0.691463	0.306210
0.6													1.089596	0.672629	0.118008
													0.523167	0.731618	0.173120
	1.0												1.119423	0.550709	0.513083
	2.0												0.532058	0.608805	0.602607
													1.138919	0.478613	0.896218
		1.0											0.537001	0.537285	1.002613
		1.5											1.100445	0.462508	0.368035
													0.526459	0.503228	0.434142
			0.5										1.097094	0.325934	0.408503
			0.8										0.525596	0.352052	0.475888
													1.076806	0.671371	0.036577
													0.519338	0.725279	0.015795
				1.0									1.056147	0.711011	0.362402
				1.5									0.512991	0.760006	0.314614
													1.094236	0.554516	0.276869
													0.524632	0.617959	0.332869
					0.3								1.090802	0.498284	0.298652
					0.5								0.523660	0.563421	0.352207
													1.107801	0.593748	0.393198
													0.527782	0.662885	0.531927
						1.3							1.114627	0.567092	0.508803
													0.529339	0.641170	0.531927
						1.5							1.147816	0.628769	0.237638
													0.540705	0.690220	0.299120
							1.0						1.147816	0.628769	0.237638
							2.0						0.553105	0.689233	0.293084
													0.577512	0.695128	0.262560
								1.0					0.389735	0.712749	0.313723
								2.0					0.148915	0.389735	0.276172
													0.245268	0.732182	0.321552
									0.4				0.395332	0.734342	0.302968
									0.7				0.306638	0.733425	0.330832
													0.134631	0.789477	0.336837
													0.088929	0.764182	0.351027
										0.5			0.134631	0.789477	0.336837
										0.9			0.593624	0.676285	0.297356
													0.134631	0.789377	0.336837
													0.655487	0.661994	0.289946
											4		1.089566	0.479765	0.305820
											5		0.523299	0.545156	0.358596
													1.083396	0.397961	0.337587
													0.521387	0.462064	0.387138
												1.0	1.102226	0.734505	0.205827
													0.526799	0.792304	0.267719
												1.5	1.104990	0.822603	0.170201
													0.527526	0.877833	0.234269
													1.095875	0.472794	0.314399
													0.522672	0.406522	0.421554
													1.094547	0.385444	0.351524
													0.522672	0.252984	0.483606

Table 2 shows how different thermophysical parameters affect the skin friction coefficient $(-f''(0))$, Nusselt number $(\theta'(0))$, and Sherwood number $(-\phi'(0))$ for Casson and Williamson nanofluids. The skin friction coefficient for Casson nanofluid is seen to consistently show slightly lower values compared to Williamson nanofluid across various parameter setting. This indicates that Casson nanofluid experiences lower fractional resistance.

It is also observed that the Williamson nanofluid experiences more friction at the boundary layer, due to the gradual shear thinning behaviour, which causes it to retain higher viscosity near the boundary layer. It is again noted that the Nusselt number for Casson nanofluid is higher compared to Williamson nanofluid due to the fluid lower viscosity, allowing for more efficient thermal energy transfer. Williamson nanofluid exhibits lower Nusselt number because of less efficient heat transfer. The viscoelastic nature of Williamson nanofluid leads to a thicker thermal boundary layer which reduces heat transfer rate.

Also, the Sherwood number for Casson nanofluid is observed to be higher compared to Williamson nanofluid due to the effective mass transfer rate of the Casson nanofluid. Furthermore, it is noted that an increase in magnetic field parameter increases the Skin friction coefficient of both nanofluids while depleting the Nusselt and Sherwood numbers due to the Lorentz force induced by magnetic field, which acts as a resistive force. Moreover, a rise in thermal Grashof number increases the skin friction coefficient, Nusselt and Sherwood numbers of both nanofluids, this is due to buoyancy forces which promote fluid motion.

Also an increase in the the Soret number was noted to decrease both the skin friction and Sherwood number of both nanofluids, with Casson nanofluid showing a larger decline, due to thermophoresis which weakens the near-wall velocity and concentration gradients. Casson nanofluid shows a stronger response because of its shear-thinning and yield stress behaviour making it more sensitive to thermophoresis effects. Lastly, it is also observed that a rise in the Eckert number rises the Skin friction coefficient, Nusselt number and Sherwood number of both Casson and Williamson Nanofluids.

3.3 Graphical Results

3.3.1 **Effects of Parameter Variation on Velocity Profiles.**

Th impact of the various thermo-physical parameters on the velocity profiles of both Casson and Williamson nanofluids are presented in Figures $2-8$. Figure 2 presents the effects of the Soret number on the velocity profiles of both Casson and Williamson nanofluids. It is noted that an increase in Soret number increases the velocity profiles of both nanofluids. Casson nanofluid shows more pronounced increase in velocity profile as the Soret number increases compared to Williamson nanofluid, thus implying that thermal diffusion increases the fluid motion significantly.

For Williamson nanofluid, the increase in velocity is gradual meaning that it is less sensitive to changes in the Soret number. Figures 3 and 4 present the effects of Thermal Grashof number and Solutal Grashof number on the velocity profiles of both Casson and Williamson nanofluids. The velocity profiles of both nanofluids increase with an increase in both thermal and Grashof numbers. But the increase in Williamson nanofluid is less pronounced compared to the Casson nanofluid, indicating that Williamson nanofluid responds less to buoyancy effects.

Again, Figure 5 presents the effects of thermophoresis parameter on velocity profiles of both Casson and Williamson nanofluids. It is observed that an increase in thermopheresis parameter increases the velocity profiles of both Casson and Williamson nanofluids, with Williamson nanofluid showing less increment compared to Casson nanofluid. This shows that thermophoresis has a stonger effect on Williamson nanofluid compared to Casson nanofluid.

Figure 6 presents the effects of nonlinear parameter on the velocity profiles of both nanofluids. It is noted that the velocity profiles of both Casson and Williamson nanofluids decrease with an increase in nonlinear parameter. The velocity decrease is less steep for Williamson nanofluid comapared to Casson nanofluid, suggesting that there is strong non-Newtonian effects on flow resistance for Casson nanofluid.

Figure 7 also presents the effects of magnetic field parameter on the velocity profiles of both Casson and Williamson nanofluids. It is observed that an increase in magnetic parameter decreases the velocity profiles of the nanofluids. The reduction is due to the Lorentz force acting on the fluid. The reduction in velocity is less pronounced for Williamson nanofluid compared to Casson nanofluid, thus suggesting that Williamson nanofluid is more sensitive to magnetic field effects. Figure 8 presents the effects of chemical reaction parameter on the velocity profiles of both Casson and Williamson nanofluids. It is noted that the velocity profiles of both Casson and Williamson nanofluids decrease with an increase in chemical reaction parameter, with Williamson nanofluid been observed to be less pronounced to decrease velocity compared to Casson nanofluid.

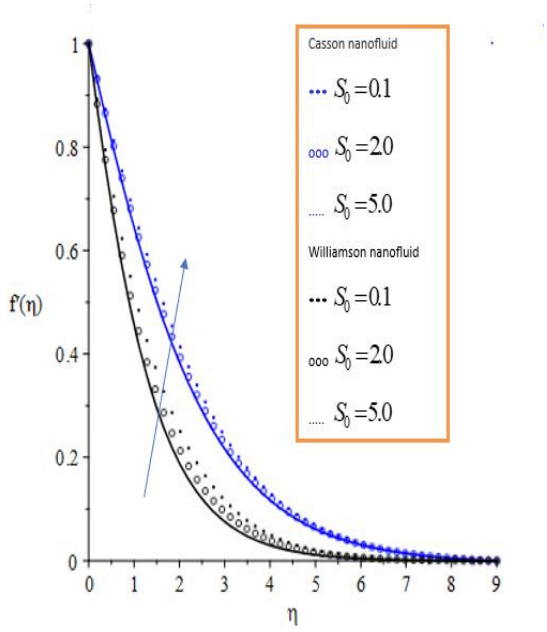

Fig. 2: Velocity profile for varying values of the Soret number with: $Pr = 3$, $Sc = 0.5$, $\beta = 0.4$, $Ec = 0.1$, $G_T = 0.1$, $We = 0.4$, $G_c = 0.1$, $R = 0.1$, $N_t = 0.2$, $N_b = 0.5$, $M = 0.1$, $D_o = 0.3$, $\omega_1 = 0.4$, and $m = 0.2$.

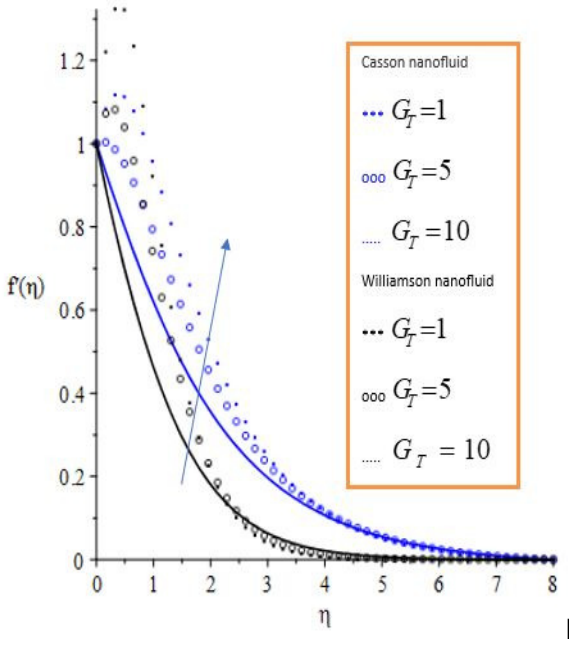

Fig. 3: Velocity Profile for varying values of Thermal Grashof number with: $Ec = 0.1$, $Sc = 0.4$, $\beta = 0.4$, $R = 0.5$, $m = 0.2$, $We = 0.4$, $G_c = 0.1$, $\omega_1 = 0.4$, $Pr = 3$,$N_t = 0.2$, $N_b = 0.5$, $D_o = 0.1$, $S_o = 0.3$, and $M = 0.1$, .

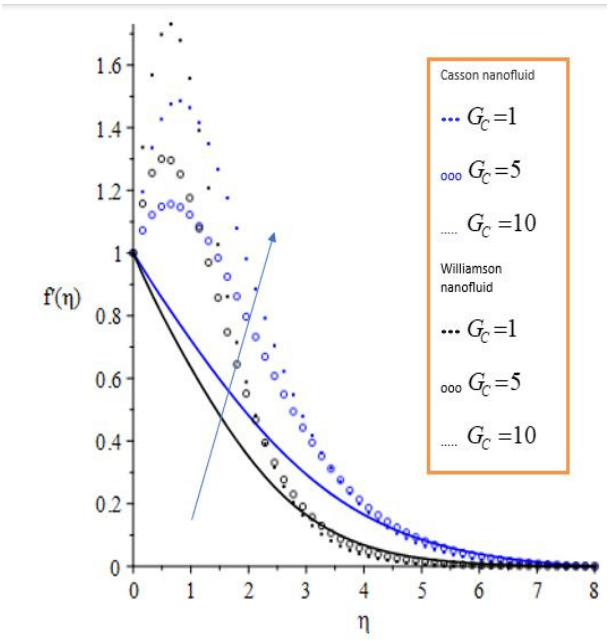

Fig. 4: Velocity Profile for varying values of Solutal Grashof number with: $Ec = 0.1$, $Sc = 0.4$, $\beta = 0.4$, $R = 0.5$, $m = 0.2$, $We = 0.4$, $G_T = 0.1$, $\omega_1 = 0.4$, $Pr = 3$,$N_t = 0.2$, $N_b = 0.5$, $D_o = 0.1$, $S_o = 0.3$, and $M = 0.1$, .:

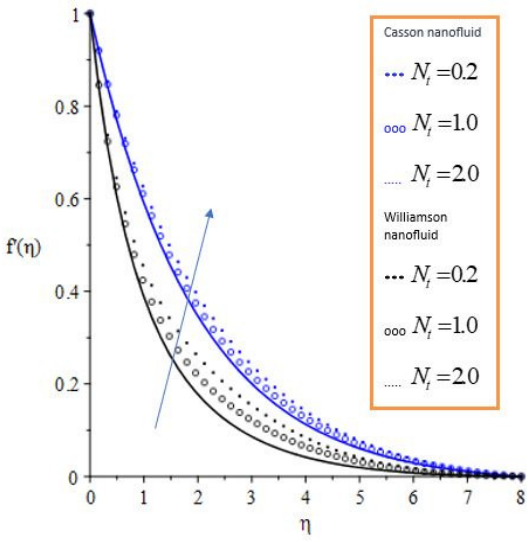

Fig. 5: Velocity Profile for varying values of Thermophoresis parameter with: $Ec = 0.1$, $Sc = 0.4$, $\beta = 0.4$, $R = 0.5$, $m = 0.2$, $We = 0.4$, $G_T = 0.1$, $G_c = 0.1$,$\omega_1 = 0.4$, $Pr = 3$, $N_b = 0.5$, $D_o = 0.1$, $S_o = 0.3$, and $M = 0.1$, .

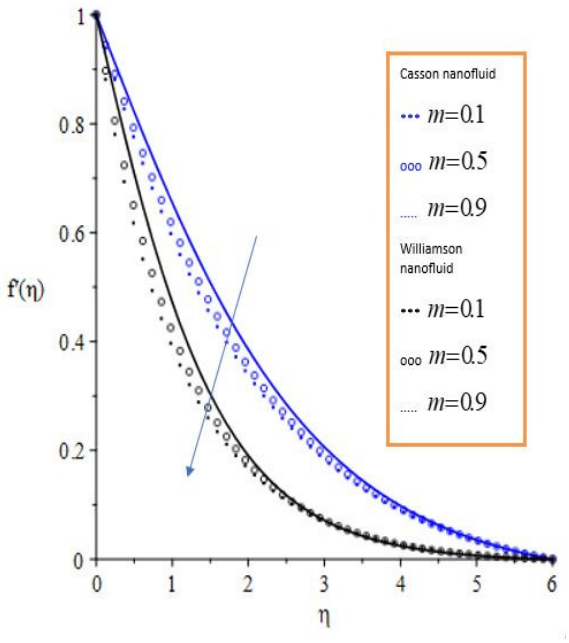

Fig. 6: Velocity Profile for varying values of nonlinear parameter with: $Ec = 0.1$, $Le = 0.4$, $\beta = 0.4$, $R = 0.5$, , $We = 0.4$, $G_T = 0.1$, $G_c = 0.1$, $\omega_1 = 0.4$, $Pr = 3$,$N_t = 0.2$, $N_b = 0.5$, $D_o = 0.1$, $S_o = 0.3$, and $M = 0.1$, .

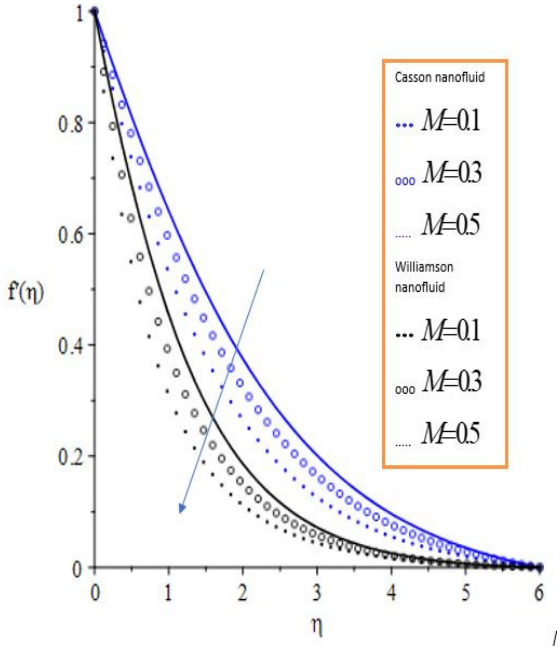

Fig. 7: Velocity Profile for varying values of magnetic field parameter with: $Ec = 0.1$, $Sc = 0.4$, $\beta = 0.4$, $R = 0.5$, $m = 0.2$, $We = 0.4$, $G_T = 0.1$, $G_c = 0.1$,$\omega_1 = 0.4$, $Pr = 3$,$N_t = 0.2$, $N_b = 0.5$, $D_o = 0.1$, $S_o = 0.3$, and $m = 0.2$, .

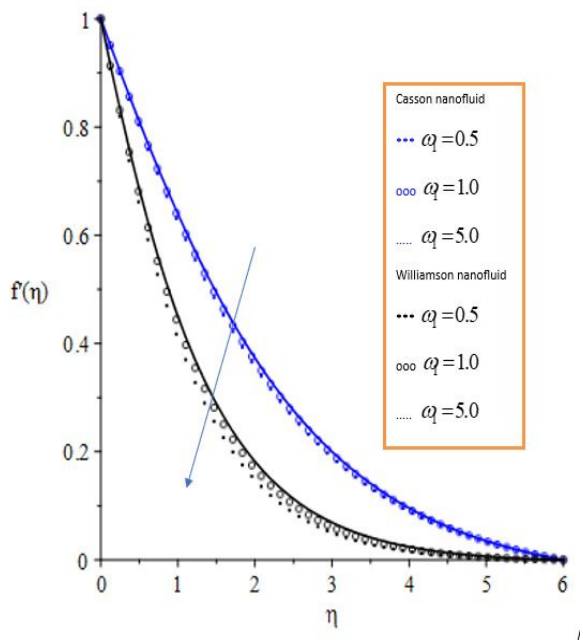

Fig. 8: Velocity Profile for varying values of rate of chemical reaction parameter with: $Ec = 0.1$, $Sc = 0.5$, $\beta = 0.4$, $R = 0.5$, $m = 0.2$, $We = 0.4$, $G_T = 0.1$, $G_c = 0.1$,$M = 0.1$, $Pr = 3$,$N_t = 0.2$, $N_b = 0.5$, $D_o = 0.1$, $S_o = 0.3$, and $m = 0.2$,

3.3.2 **Effects of Parameter Variation on Temperature Profiles**

The impact of various thermo-physical parameters on the temperature profiles of both Casson and Williamson nanofluids are presented in Figures 9 – 18. Figure 9 presents the effects of Soret number on temperature profiles of both Casson and Williamson nanofluid. An increase in Soret number is observed to increase the temperature profiles of both nanofluids, with Williamson nanofluid indicating less increment compared to Casson nanofluid. The increase in temperature of both fluid is as a result of Soret number intensifying the coupling between thermal and concentration fields. Figure 10 presents the effects of Dufour number on temperature profiles of both Casson and Wiliamson nanofluids. It has been seen that a rise in Duffour number increases the temperature profiles of both nanofluids, with Williamson nanofluid showing less incement in temperature compared to Casson nanofluid. This means that Casson nanofluid is more sensitive to Dufour effects than Williamson nanofluid and this is due to strong thermal diffusion effects due to concentration gradients. Also, Figure 11 presents the effects of radiation parameter on temperature profiles of both Casson and Williamson nanofluids. It is observed that an increase in the radiation parameter increases the temperature profiles of both nanofluids. The temperature increase for Williamson nannofluid is less pronounced

compared to Casson nanofluid. This means that Casson nanofluid is more affected by radiative heat transfer. Figure 12 presents the effects of Brownian motion parameter on temperature profiles of both Casson and Williamson nanofluids. It is noted that an increase in Brownian motion parameter raises the temperature profiles of both nanofluids. Williamson nanofluid effect with temperature increase is milder compared to Casson nanofluid. This means that nanoparticle-induced thermal fluctuations strongly impact the Casson nanofluid with increased Brownian motion parameter.

Figure 13 also, presents effects of magnetic field parameter on temperature profiles of both Casson and Williamson nanofluids. It is again noted that a rise in magnetic field parameter increases the temperature profiles of both nanofluids, with Williamson nanofluid showing less pronounced changes to temperature increase compared to Casson nanofluid. The rise in the temperature profiles suggest that magnetic forces enhance heat distribution especially in Casson nanofluid. Figure 14 presents the effects of Eckert number on temperature profiles of both Casson and Williamson nanofluids. It is again noted that an increase in Eckert number raises the temperature profiles of both Casson and Williamson nanofluids, with Casson nanofluid showing more impact to the temperature increase compared with Williamson nanofluid. This suggests that viscous dissipation generate more heat in Casson nanofluid while for Williamson nanofluid viscous dissipation effect is lower as Eckert number rises. Figure 15 also presents the effects of nonlinear parameter on the temperature profiles of both Casson and Williamson nanofluids. It is also observed that an increase in nonlinear parameter increases the temperature profiles of both nanofluids, with Casson nanofluid showing greater impact compared to Williamson nanofluid. This increase in temperature is as a result of non-Newtonian effects.

Figures 16 and 17 present the effects of thermal Grashof number and Solutal Grashof number on the temperature profiles of both Casson and Williamson nanofluids. It is noted that an increase in both thermal and Grashof numbers reduce the temperature profiles of both nanofluids, with Casson nanofluid showing more impact to temperature decrease compared to Williamson nanofluid. The reduction in the temperature profiles of both nanofluids is as a result of buoyancy-driven convection. Lastly, Figure 18 shows the effects of Prandtl number on temperature profiles of both Casson and Williamson nanofluids. It is again, noted that an increase in Prandtl number reduces the temperature profiles of both nanofluids, with Casson nanofluid showing greater impact with the temperature decrease compared to Williamson nanofluid. The decrease is due to higher viscosity lowering the thermal diffusion.

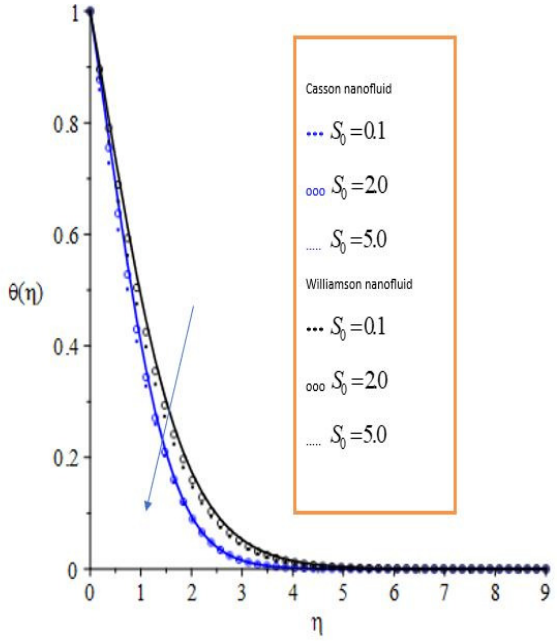

Fig. 9: Temperature Profile for varying values of Soret number with:$Ec = 0.1$, $Sc = 0.5$, $\beta = 0.4$, $R = 0.5$, $m = 0.2$, $We = 0.4$, $G_T = 0.1$, $G_c = 0.1$,$M = 0.1$, $Pr = 3$,$N_t = 0.2$, $N_b = 0.5$, $D_o = 0.1$, $\omega_1 = 0.4$ and $m = 0.2$,

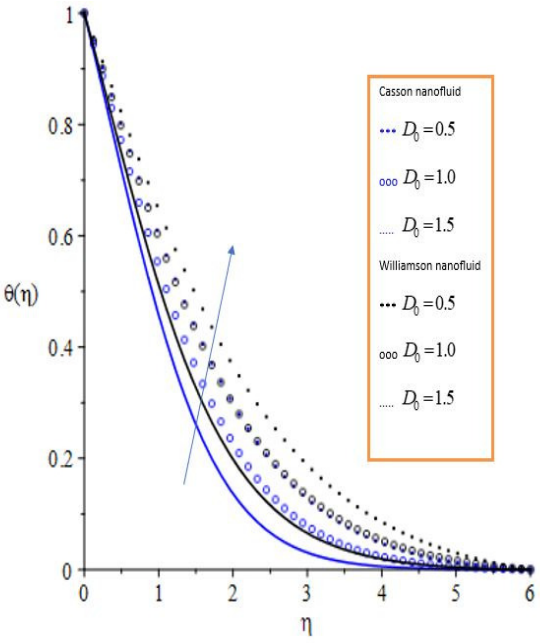

Fig. 10: : Temperature Profile for varying values of Dufour number with: $Ec = 0.1$, $Sc = 0.5$, $\beta = 0.4$, $R = 0.5$, $m = 0.2$, $We = 0.4$, $G_T = 0.1$, $G_c = 0.1$,$M = 0.1$, $Pr = 3$,$N_t = 0.2$, $N_b = 0.5$, $S_o = 0.3$, $S_o = 0.3$, $\omega_1 = 0.4$ and $m = 0.2$,

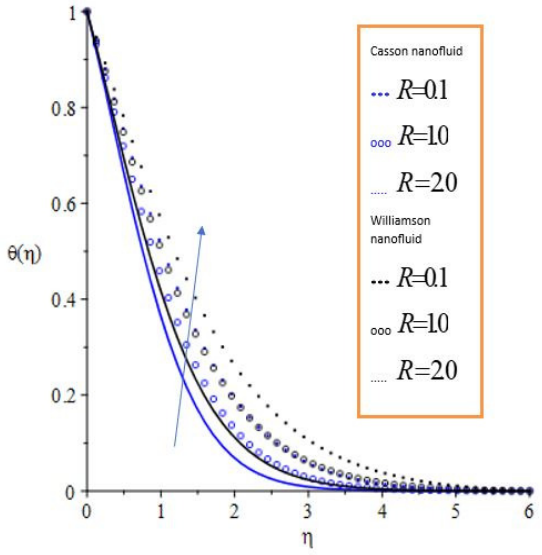

Fig. 11: Temperature Profile for varying values of Radiation parameter with: $Ec = 0.1$, $Sc = 0.5$, $\beta = 0.4$, $D_o = 0.3$, $m = 0.2$, $We = 0.4$, $G_T = 0.1$, $G_c = 0.1$,$M = 0.1$, $Pr = 3$,$N_t = 0.2$, $N_b = 0.5$, $D_o = 0.1$, $S_o = 0.3$, $\omega_1 = 0.4$ and $m = 0.2$,

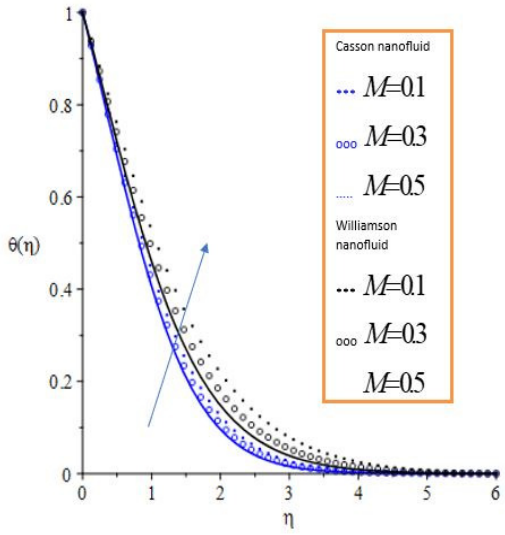

Fig. 13: Temperature Profile for varying values of magnetic field parameter with: $Ec = 0.1$, $Sc = 0.5$, $\beta = 0.4$, $R = 0.5$, $m = 0.2$, $We = 0.4$, $G_T = 0.1$, $G_c = 0.1$,$N_b = 0.5$, $Pr = 3$,$N_t = 0.2$, $N_b = 0.5$, $D_o = 0.1$, $S_o = 0.3$, $\omega_1 = 0.4$ and $m = 0.2$,

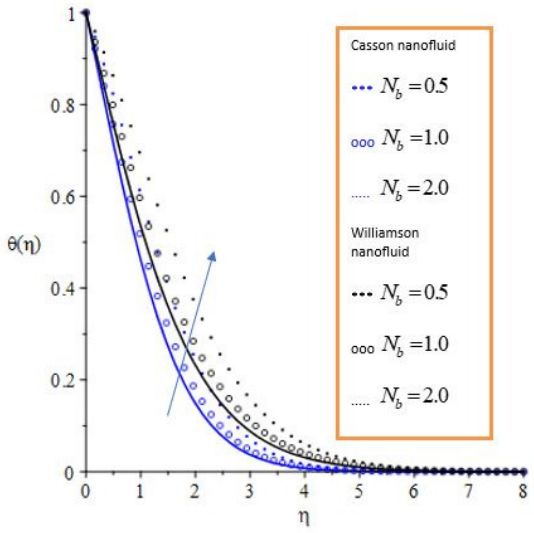

Fig. 12: Temperature Profile for varying values of Brownian motion parameter with: $Ec = 0.1$, $Sc = 0.5$, $\beta = 0.4$, $R = 0.5$, $m = 0.2$, $We = 0.4$, $G_T = 0.1$, $G_c = 0.1$,$M = 0.1$, $Pr = 3$,$N_t = 0.2$, $R = 0.5$, $D_o = 0.1$, $S_o = 0.3$, $\omega_1 = 0.4$ and $m = 0.2$,

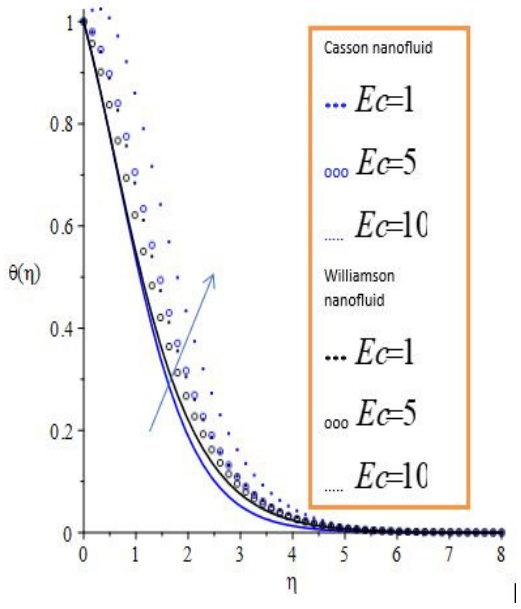

Fig. 14: Temperature Profile for varying values of Eckert number with: $M = 0.1$, $Sc = 0.5$, $\beta = 0.4$, $R = 0.5$, $m = 0.2$, $We = 0.4$, $G_T = 0.1$, $G_c = 0.1$,$M = 0.1$, $Pr = 3$,$N_t = 0.2$, $N_b = 0.5$, $D_o = 0.1$, $S_o = 0.3$, $\omega_1 = 0.4$ and $m = 0.2$,

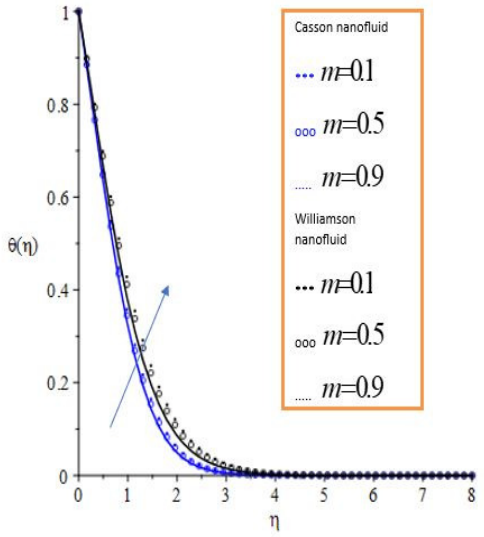

Fig. 15: Temperature Profile for varying values of nonlinear parameter: $Ec = 0.1$, $Sc = 0.5$, $\beta = 0.4$, $R = 0.5$, $m = 0.2$, $We = 0.4$, $G_T = 0.1$, $G_c = 0.1$,$M = 0.1$, $Pr = 3$,$N_t = 0.2$, $N_b = 0.5$, $D_o = 0.1$, $S_o = 0.3$,$\omega_1 = 0.4$ and $Ec = 0.2$,

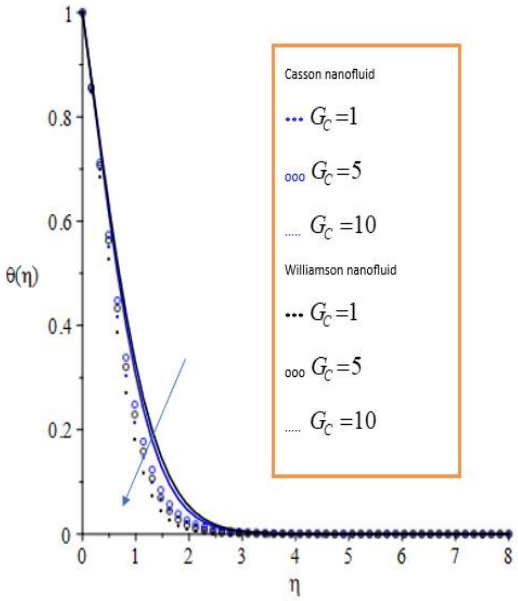

Fig. 17: Temperature Profile for varying values of Solutal Grashof number with: $Ec = 0.1$, $Sc = 0.5$, $\beta = 0.4$, $R = 0.5$, $m = 0.2$, $We = 0.4$, $G_T = 0.1$, ,$M = 0.1$, $Pr = 3$,$N_t = 0.2$, $N_b = 0.5$, $D_o = 0.1$, $S_o = 0.3$, $\omega_1 = 0.4$ and $m = 0.2$,

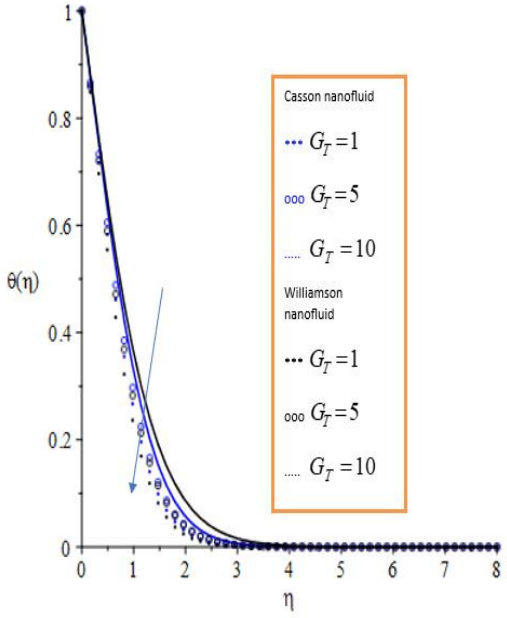

Fig. 16: Temperature Profile for varying values of Thermal Grashof number with: $Ec = 0.1$, $Sc = 0.5$, $\beta = 0.4$, $R = 0.5$, , $We = 0.4$, $m = 0.2$, $G_c = 0.1$,$M = 0.1$, $Pr = 3$,$N_t = 0.2$, $N_b = 0.5$, $D_o = 0.1$, $S_o = 0.3$, $\omega_1 = 0.4$ and $m = 0.2$,

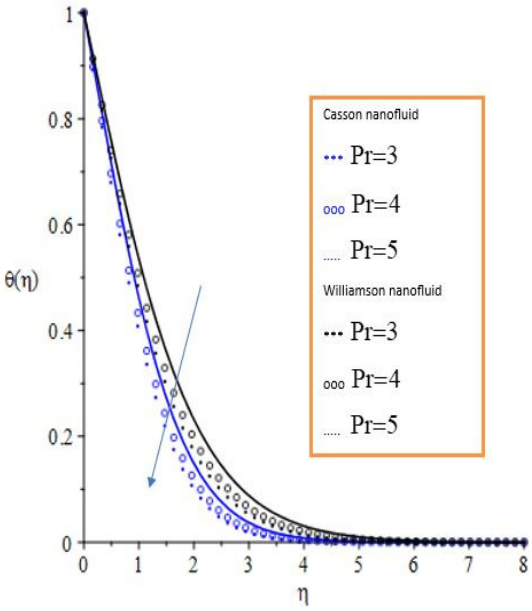

Fig. 18: Temperature Profile for varying values of Prandtl number with: $Ec = 0.1$, $Sc = 0.5$, $\beta = 0.4$, $R = 0.5$, $m = 0.2$, $We = 0.4$, $G_T = 0.1$, $G_c = 0.1$,$M = 0.1$, $N_t = 0.2$, $N_b = 0.5$, $D_o = 0.1$, $S_o = 0.3$, $\omega_1 = 0.4$ and $m = 0.2$,

3.3.3 **Effects of Parameter Variations on Concentration Profiles**

The impact of various thermo-physical parameters on the Concentration profiles of both Casson and Williamson nanofluids are presented in Figures 19 – 30. Figure 19 presents the effects of the Soret number on concentration profiles of both Casson and Williamson nanofluid. It is observed that an increase in Soret number increases the concentration profiles of both nanofluids, with Casson nanofluid showing significant temperature increase compared to Williamson nanofluid. This is as a result of strong thermal diffusion effects on mass transfer. Figure 20 presents the effects of nonlinear parameter on the concentration profiles of both Casson and Williamson nanofluids. It is observed that an increase in nonlinear parameter increases the concentration profiles of both nanofluids, with the increase for Williamson nanofluid been more pronounced compared to Casson nanofluid. The increase is due to suppression of mass transfer due to non-Newtonian effects. Again, Figure 21 presents the effects of Thermophoresis parameter on the concentration profiles of both Casson and Williamson nanofluids. It is noted that an increase in thermophoresis parameter leads to an increase in concentration profiles of both nanofluids, with the increase in concentration of Casson nanofluid pronouncing greater impact compared to Williamson nanofluid. The increase is due to particle movement as a result of temperature gradient. Figure 22 presents the effects of magnetic field parameter on the concentration profiles of both Casson and Williamson nanofluids. It is noted that a raise in magnetic field paramter increases the concentration profiles of both nanofluids, with the increase been less severe in Williamson nanofluid compared to Casson nanofluid. This is due to Williamson nanofluid gradual shear-thinning behaviour and lower sensitivity stress and shear rate changes. Figures 23 and 24 present the effects of thermal Grashof number and Solutal Grashof number on the concentration profiles of both Casson and Williamson nanofluids. It is observed that an increase in Thermal Grashof and Solutal numbers decrease the concentration profiles of both nanofluids, with the decrease in concentration of Williamson nanofluid been less pronounced compared to Casson nanofluid. The reduction in concentration of both nanofluids is as a result of mass diffusion due to buoyancy-driven flow and convective mass transfer. Figure 25 presents the effects of Brownian motion parameter on concentration profiles of both Casson and Williamson nanofluids. It has been noted that a rise in Brownian motion parameter decreases the concentration profiles of both nanofluids, with the reduction in Williamson nanofluid been milder compared to Casson nanofluid. The decrease in concentration is as a result of strong nanoparticles effects on mass transfer. The effects of the Eckert number on concentration profiles of both Casson and Williamson nanofluids are presented in Figure 26. It is observed that an increase in Eckert number decreases the concentration profiles of both nanofluids, with the decrease in concentration of Casson nanofluid been more rapid compared to Williamson nanofluid due to viscous dissipation. Figure 27 presents the effects of radiation parameter on concentration profiles of both Casson and Williamson nanofluids. It is observed that a rise in radiation parameter decreases the concentration profiles of both nanofluids, with Casson nanofluid again showing greater decrease in concentration compared to Williamson nanofluid due to species distribution in the nanofluid. The effects of chemical reaction parameter on the concentration profiles of both Casson and Williamson nanofluids are also illustrated in Figure 28. It is noted that the concentration profiles of both nanofluids also decrease with an increase in chemical reaction parameter, Casson nanofluid again shows tremendous decrease in concentration compared to Williamson nanofluid, This shows that chemical reaction reduces species concentration more srongly for Casson nanofluid. Again, Figure 29 presents the effects of Dufour parameter on concentration profiles of both Casson and Williamson nanofluids. It is noted that an increase in Dufour parameter decreases the concentration profiles of both nanofluids, with Casson nanofluid having greater impact on the decrease in concentration compared to Williamson nanofluid. The decrease is due to strong thermophoretic effects on mass transfer. Finally, Figure 30 presents the effects of Schmidt number on the concentration profiles of both Casson and Williamson nanofluids. It is again noted that an increase in Schmidt number reduces the the concentration profiles of both nanofluids, with Casson nanofluid showing more pronounced concentration decrease compared to Williamson nanofluid.

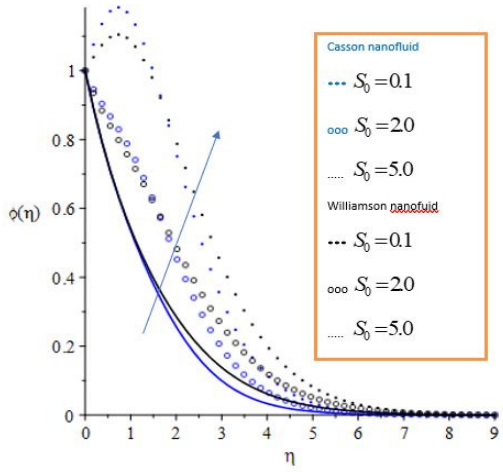

Fig. 19: Concentration Profile for varying values of Soret number with: $Ec = 0.1$, $Sc = 0.5$, $\beta = 0.4$, $R = 0.5$, $m = 0.2$, $We = 0.4$, $G_T = 0.1$, $G_c = 0.1$,$M = 0.1$, $Pr = 3$,$N_t = 0.2$, $N_b = 0.5$, $D_o = 0.1$, $\omega_1 = 0.4$ and $m = 0.2$,

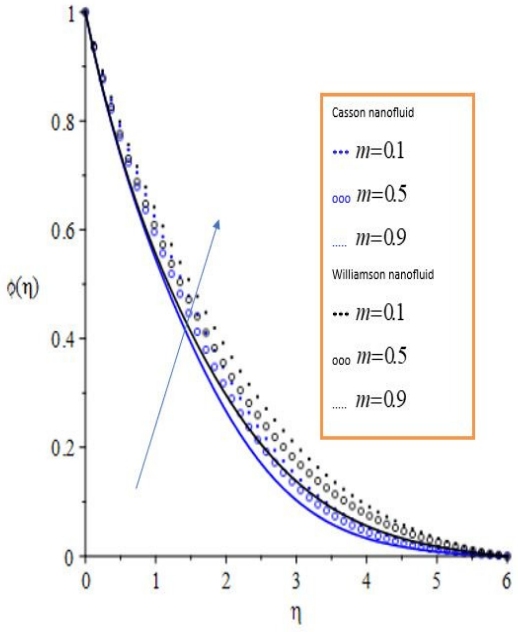

Fig. 20: Concentration Profile for varying values of nonlinear parameter with: $Ec = 0.1$, $Sc = 0.5$, $\beta = 0.4$, $R = 0.5$, $m = 0.2$, $We = 0.4$, $G_T = 0.1$, $G_c = 0.1$,$M = 0.1$, $Pr = 3$,$N_t = 0.2$, $N_b = 0.5$, $D_o = 0.1$, $\omega_1 = 0.4$ and $S_o = 0.3$,

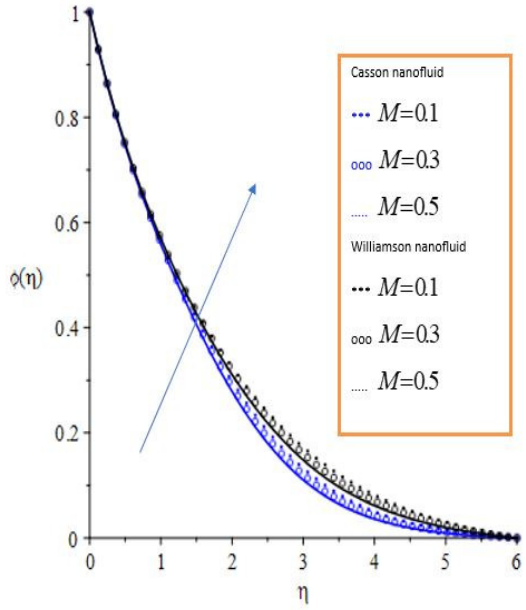

Fig. 22: Concentration Profile for varying values of magnetic field parameter with: $Ec = 0.1$, $Sc = 0.5$, $\beta = 0.4$, $R = 0.5$, $m = 0.2$, $We = 0.4$, $G_T = 0.1$, $G_c = 0.1$, $Pr = 3$,$N_t = 0.2$, $N_b = 0.5$, $D_o = 0.1$, $S_o = 0.3$, $\omega_1 = 0.4$ and $m = 0.2$.

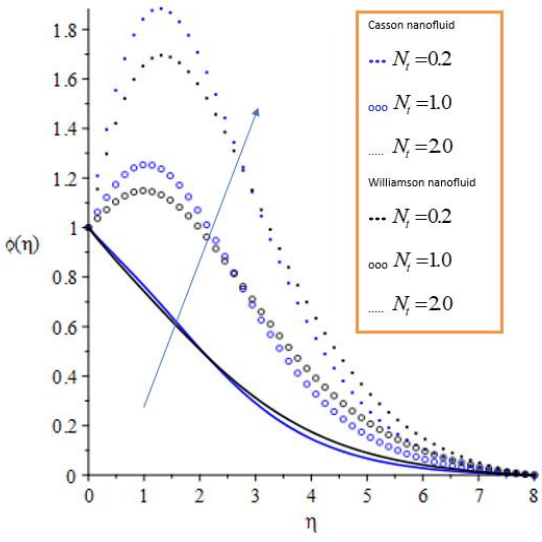

Fig. 21: Concentration Profile for varying values of Thermophoresis parameter with: $Ec = 0.1$, $Sc = 0.5$, $\beta = 0.4$, $R = 0.5$, $m = 0.2$, $We = 0.4$, $G_T = 0.1$, $G_c = 0.1$,$M = 0.1$, $Pr = 3$, $N_b = 0.5$, $D_o = 0.1$, $S_o = 0.3$, $\omega_1 = 0.4$ and $m = 0.2$.

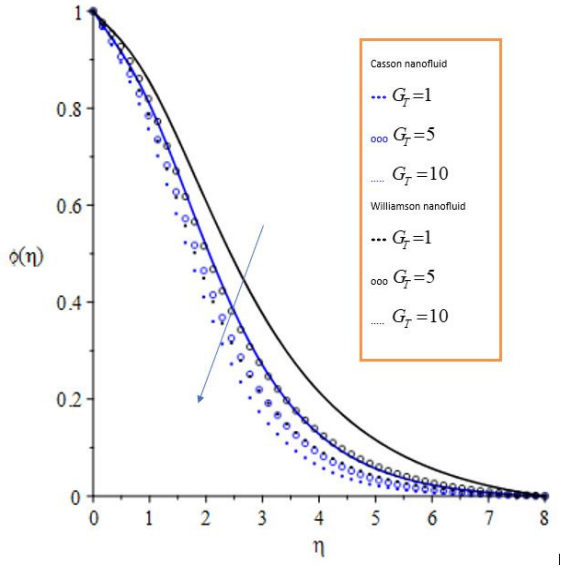

Fig. 23: Concentration Profile for varying values of Thermal Grashof number with: $Ec = 0.1$, $Sc = 0.5$, $\beta = 0.4$, $R = 0.5$, $m = 0.2$, $We = 0.4$, $G_c = 0.1$,$M = 0.1$, $Pr = 3$,$N_t = 0.2$, $N_b = 0.5$, $D_o = 0.1$, $S_o = 0.3$, $\omega_1 = 0.4$ and $m = 0.2$,

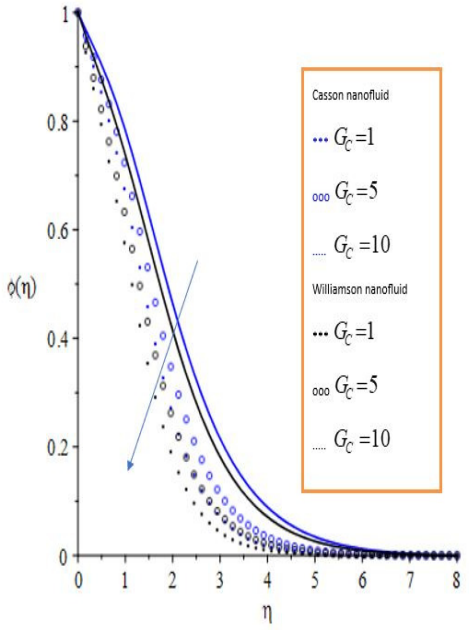

Fig. 24: Concentration Profile for varying values of Solutal Grashof number with: $Ec = 0.1$, $Sc = 0.5$, $\beta = 0.4$, $R = 0.5$, $m = 0.2$, $We = 0.4$, $G_T = 0.1$, $M = 0.1$, $Pr = 3$,$N_t = 0.2$, $N_b = 0.5$, $D_o = 0.1$, $S_o = 0.3$, $\omega_1 = 0.4$ and $m = 0.2$,

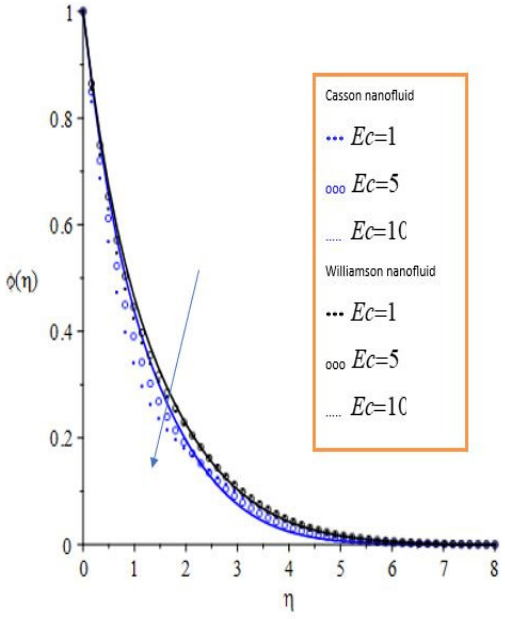

Fig. 26: Concentration Profile for varying values of Eckert number with: $Sc = 0.5$, $\beta = 0.4$, $R = 0.5$, $m = 0.2$, $We = 0.4$, $G_T = 0.1$, $G_c = 0.1$,$M = 0.1$, $Pr = 3$,$N_t = 0.2$, $N_b = 0.5$, $D_o = 0.1$, $S_o = 0.3$, $\omega_1 = 0.4$ and $m = 0.2$.

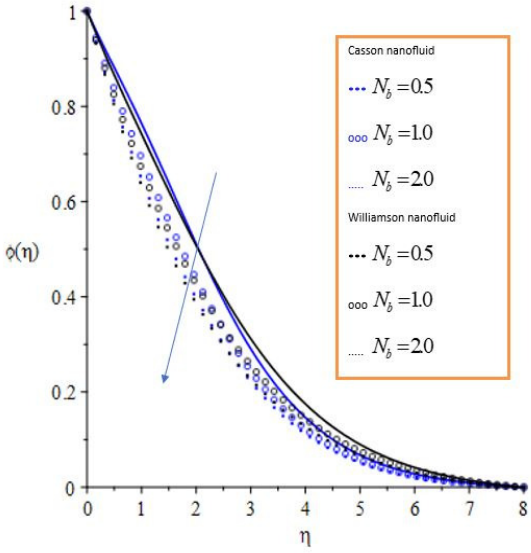

Fig. 25: Concentration Profile for varying values of Brownian motion parameter with: $Ec = 0.1$, $Sc = 0.5$, $\beta = 0.4$, $R = 0.5$, $m = 0.2$, $We = 0.4$, $G_T = 0.1$, $G_c = 0.1$,$M = 0.1$, $Pr = 3$,$N_t = 0.2$, $D_o = 0.1$, $S_o = 0.3$, $\omega_1 = 0.4$and $m = 0.2$,

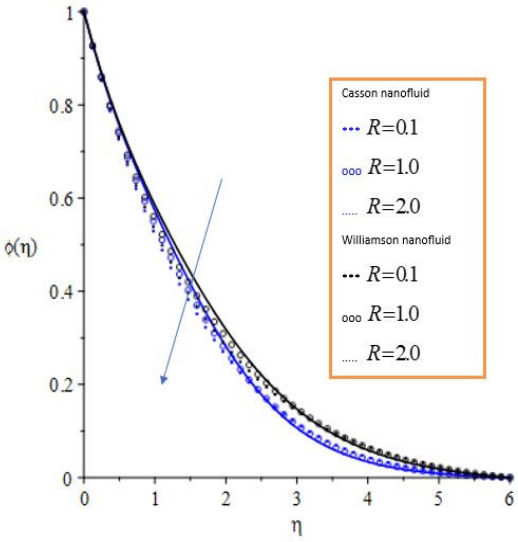

Fig. 27: Concentration Profile for varying values of Radiation parameter with: $Ec = 0.1$, $Sc = 0.5$, $\beta = 0.4$, $m = 0.2$, $We = 0.4$, $G_T = 0.1$, $G_c = 0.1$,$M = 0.1$, $Pr = 3$,$N_t = 0.2$, $N_b = 0.5$, $D_o = 0.1$, $S_o = 0.3$, $\omega_1 = 0.4$ and $m = 0.2$,

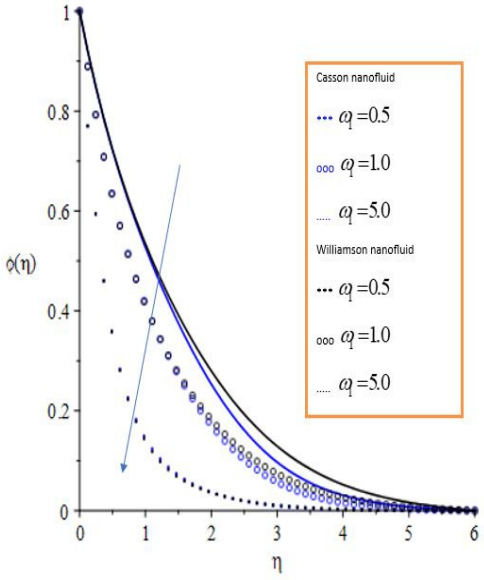

Fig. 28: Concentration Profile for varying values of rate of chemical reaction parameter with: $Ec = 0.1$, $Sc = 0.5$, $\beta = 0.4$, $R = 0.5$, $m = 0.2$, $We = 0.4$, $G_T = 0.1$, $G_c = 0.1$,$M = 0.1$, $Pr = 3$,$N_t = 0.2$, $N_b = 0.5$, $D_o = 0.1$, $S_o = 0.3$, and $m = 0.2$.

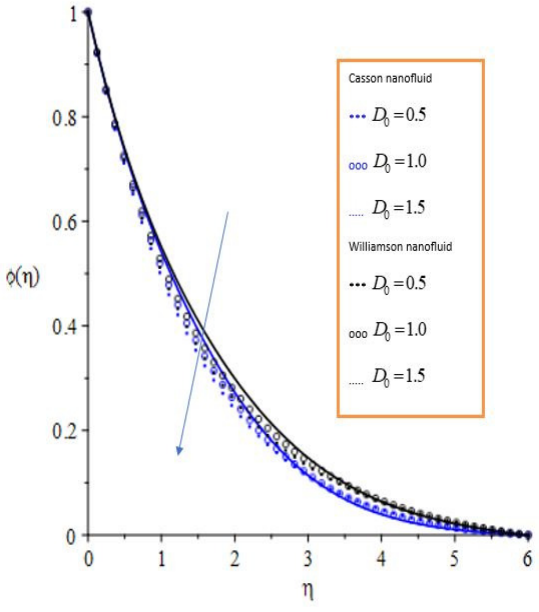

Fig. 29: Concentration Profile for varying values of Dufour number with: $Ec = 0.1$, $Sc = 0.5$, $\beta = 0.4$, $R = 0.5$, $m = 0.2$, $We = 0.4$, $G_T = 0.1$, $G_c = 0.1$,$M = 0.1$, $Pr = 3$,$N_t = 0.2$, $N_b = 0.5$, $S_o = 0.3$, $\omega_1 = 0.4$ and $m = 0.2$,

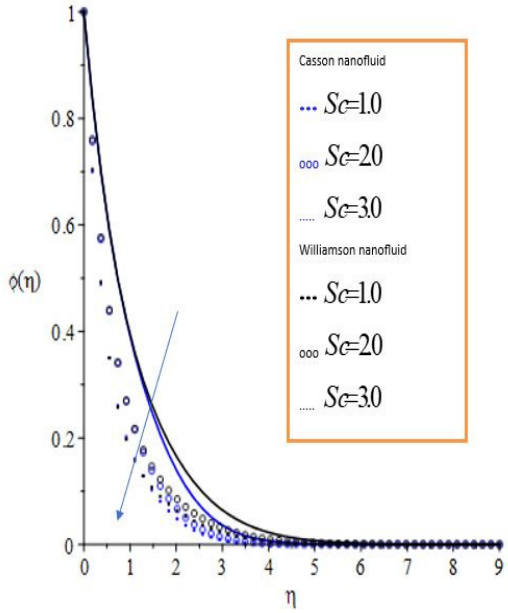

Fig. 30: Concentration Profile for varying values of Schmidt number with: $Ec = 0.1$, $\beta = 0.4$, $R = 0.5$, $m = 0.2$, $We = 0.4$, $G_T = 0.1$, $G_c = 0.1$,$M = 0.1$, $Pr = 3$,$N_t = 0.2$, $N_b = 0.5$, $D_o = 0.1$, $S_o = 0.3$, $\omega_1 = 0.4$ and $m = 0.2$,

4 Conclusions

Impact of cross diffusion on MHD flow of Casson-Williamson nanofluid past a reactive stretching surface has been investigated. The resulting model was converted into nonlinear differential equations using similarity transformation and addressed with computational techniques such as the fourth-order Runge-Kutta method and Newton-Raphson shooting technique. It has been established that Casson nanofluid is better in terms of heat transfer compared to Williamson nanofluid. The following general conclusions can be made:

i. An increase in Soret number, Dufour number and Radiation parameter appreciate the temperature profiles of both Casson and Williamson nanofluids.
ii. The velocity profiles of both Casson and Williamson nanofluids decrease with an increase in chemical reaction parameter.
iii. A rise in Soret number is observed to enhance the temperature profiles of both nanofluids, with Williamson nanofluid been less pronounced compared to Casson fluid
iv. It is noted that a rise in the radiation parameter rises the temperature profiles of both Casson and Williamson nanofluids, with the temperature increase for Williamson been less pronounced compared to Casson nanofluid.

Acknowledgment

The authors gratefully acknowledge Sohag Journal of Mathematics for providing a full waiver of the publication fee, which made the publication of this research possible. We also appreciate the editorial team for their valuable support and consideration.

References

[1] R. Cortell, Heat and fluid flow due to non-linearly stretching surfaces, *Applied Mathematics and Computation* **217**(19), 7564–7572 (2011), Elsevier.

[2] C. J. Etwire and Y. I. Seini, Radiative MHD flow over a vertical plate with convective boundary condition, *American Journal of Applied Mathematics*, Science Publishing Group (2014).

[3] B. C. Prasannakumara, N. S. Shashikumar, and P. Venkatesh, Boundary layer flow and heat transfer of fluid particle suspension with nanoparticles over a nonlinear stretching sheet embedded in a porous medium, *Nonlinear Engineering* **6**(3), 179–190 (2017), De Gruyter.

[4] A. Rasheed and M. S. Anwar, Numerical computations of fractional nonlinear Hartmann flow with revised heat flux model, *Computers & Mathematics with Applications* **76**(10), 2421–2433 (2018), Elsevier.

[5] D. Pal and N. Roy, Role of Brownian motion and nonlinear thermal radiation on heat transfer of a Casson nanofluid over a stretching sheet with slip velocity and non-uniform heat source/sink, *Journal of Nanofluids* **8**(3), 556–568 (2019), American Scientific Publishers.

[6] P.P. Humane, V.S. Patil, and A.B. Patil, Chemical reaction and thermal radiation effects on magnetohydrodynamics flow of Casson-Williamson nanofluid over a porous stretching surface, Proc. Inst. Mech. Eng. Part E: J. Process Mech. Eng. **235**(6), 2008–2018 (2021).

[7] C. J. Etwire, I. Y. Seini, and O. D. Makinde, Magnetized flow of electrically induced Maxwell nanofluid over reactive stretching plate with thermal stratification, *Earthline Journal of Mathematical Sciences* **10**(2), 241–270 (2022).

[8] M. Irfan, P. Sunthrayuth, A. Ali Pasha, M. S. Anwar, and W. A. Khan, Phenomena of thermo-solutal time's relaxation in mixed convection Carreau fluid with heat sink/source, *Waves in Random and Complex Media*, 1–13 (2022), Taylor & Francis.

[9] M. Jawad, Z. Khan, E. Bonyah, and R. Jan, Analysis of hybrid nanofluid stagnation point flow over a stretching surface with melting heat transfer, *Mathematical Problems in Engineering* **2022**(1), 9469164 (2022), Wiley Online Library.

[10] J. Hasnain and N. Abid, Numerical investigation for thermal growth in water and engine oil-based ternary nanofluid using three different shaped nanoparticles over a linear and nonlinear stretching sheet, *Numerical Heat Transfer, Part A: Applications* **83**(12), 1365–1376 (2023), Taylor & Francis.

[11] M. Khan, A. Rasheed, and M. S. Anwar, Numerical analysis of nonlinear time-fractional fluid models for simulating heat transport processes in porous medium, *ZAMM-Journal of Applied Mathematics and Mechanics/Zeitschrift für Angewandte Mathematik und Mechanik* **103**(9), e202200544 (2023), Wiley Online Library.

[12] N. Tarakaramu, P. V. Satya Narayana, N. Sivakumar, D. Harish Babu, and K. Bhagya Lakshmi, Convective conditions on 3D magnetohydrodynamic (MHD) non-Newtonian nanofluid flow with nonlinear thermal radiation and heat absorption: a numerical analysis, *Journal of Nanofluids* **12**(2), 448–457 (2023), American Scientific Publishers.

[13] Zeeshan, I. Khan, S. M. Eldin, S. Islam, and M. U. Khan, Two-dimensional nanofluid flow impinging on a porous stretching sheet with nonlinear thermal radiation and slip effect at the boundary enclosing energy perspective, *Scientific Reports* **13**(1), 5459 (2023), Nature Publishing Group UK London.

[14] U. Hayat, S. Shaiq, K. S. Nisar, A. Shahzad, A. Farooq, M. Kamran, and N. A. Shah, Comparative study of copper nanoparticles over radially stretching sheet with water and silicone oil, *Nanotechnology Reviews* **13**(1), 20230200 (2024), De Gruyter.

[15] Y. Namala, D. Hymavathi, R. Kune, and B. S. Reddy, Joint Effect of Velocity Slip and Joule Heating MHD Casson-Williamson Nanofluid Passes Through the Stretching Porous Medium, *Journal of Advanced Research in Fluid Mechanics and Thermal Sciences* **123**(1), 156–171 (2024).

[16] A. Rehman, M. C. Khun, M. Inc, L. Ragoub, S. Rezapour, and T. Muhammad, Analytical analysis of water and engine oil base nanofluid flow with the influence of viscous dissipation and variable viscosity on stretching surface, *ZAMM-Journal of Applied Mathematics and Mechanics/Zeitschrift für Angewandte Mathematik und Mechanik*, e202300773 (2024), Wiley Online Library.

[17] S. Sagheer, R. Razzaq, and U. Farooq, Non-similar analysis of heat generation and thermal radiation on Eyring-Powell Hybrid nanofluid flow across a stretching surface, *Advances in Mechanical Engineering* **16**(10), 16878132241282562 (2024), SAGE Publications Sage UK: London, England.

[18] H. Ullah, S. A. Abas, M. Fiza, I. Khan, A. A. Rahimzai, and A. Akgul, A numerical study of heat and mass transfer characteristic of three-dimensional thermally radiated bi-directional slip flow over a permeable stretching surface, *Scientific Reports* **14**(1), 19842 (2024), Nature Publishing Group UK London.

[19] C. J. Etwire, I. Y. Seini, R. Musah, and O. D. Makinde, Chemical Reaction and Cross Diffusion Effects on Heat and Mass Transfer Characteristics of Viscoelastic Oil-Based Nanofluid Over a Porous Nonlinear Stretching Surface, *Earthline Journal of Mathematical Sciences* **15**(1), 35–58 (2025).

[20] M. J. Fuseini and C. J. Etwire, Effects of Non-uniform Heat Generation on Magnetized Casson-Williamson Nanofluid Flow Towards a Dissipative Stagnation Point, (2025).

Biography

Christian John Etwire is a senior lecturer and the Head of Department of Mathematics at C. K. Tedam University of Technology and Applied Sciences, Ghana. He received his PhD degree in Mathematics from the University for Development Studies, Ghana. His research interests include: computational fluid dynamics, mathematical modelling and optimization. He has published several research articles in reputable mathematical and engineering journals.

Fuseini John Mathias is a masters student in mathematics at C. K. Tedam University of Technology and Applied Sciences, Ghana.